Journal of the Indian Chemical Society 101 (2024) 101423

Contents lists available at ScienceDirect

Journal of the Indian Chemical Society

journal homepage: www.journals.elsevier.com/journal-of-the-indian-chemical-society

A sustainable strategy to improve photocatalytic degradation properties of CuO and CuO-rGO nanocomposite using *Eucalyptus* leaf extract

S. Satheeskumar [a,*], S. Surendhiran [a], C. Shanthi [b], A. Panneerselvam [c], S. Senthilkumar [d], B.V. Bhuvaneswari [e]

[a] Centre for Nanoscience and Technology, KS Rangasamy College of Technology, Tiruchengode, 637 215, Tamilnadu, India
[b] Department of Physics, Sona College of Technology, Salem, 636 005, Tamilnadu, India
[c] Department of Physics, Vivekanandha College of Engineering for Women (Autonomous) Elayampalayam, Tiruchengode, 637 205, Namakkal, Tamil Nadu, India
[d] Department of Science, ST.Xaviers College, Jaipur, 302029, Rajasthan, India
[e] Department of Physics, Alagappa Chettiar Government College of Engineering and Technology, Karaikudi, 630 003, Tamilnadu, India

ARTICLE INFO

Keywords:
CuO-rGO nanocomposite
Eucalyptus leaves extract
Hydrothermal
Rhodamine B
Rose Bengal
Pollution control

ABSTRACT

In this study, Copper oxide (CuO) nanoparticles were synthesized using a sustainable approach. The process comprised *Eucalyptus* leaf extract as both a biological capping agent and a reducing agent. The synthesis process used a one-pot hydrothermal technique to efficiently combine CuO nanoparticles with reduced graphene oxide (rGO). Analytical methods were utilized to investigate the prepared nanocomposite's structural, crystalline, morphological, functional, optical, and thermal characteristics. The prepared sample was analyzed using X-ray diffraction, which revealed that CuO nanoparticles have a monoclinic crystal structure, and no impurity peaks were observed. Field emission scanning microscopes displayed the uniform dispersion of spherical CuO nanoparticles with layered and non-agglomerated, resembling a sponge-like structure of rGO. The microstructural analysis also confirmed the dispersion of copper inside reduced graphene oxide (rGO) sheets. The optical properties, including light absorption and bandgap width, were investigated using UV–visible spectroscopy using bandgap energies of 2.5 and 2.8 eV. In addition, the nanocomposite's ability to degrade cationic Rhodamine 6G and anionic Rose Bengal dyes by photocatalysis was evaluated. The degradation of RB and Rh6G dyes was characterized by nanocatalysis using UV–visible spectroscopy and a pseudo-first-order kinetics model. The pseudo-first-order degradation kinetic rate of Rhodamine 6G was determined to be 2.55 x 10^{-2} min^{-1}, indicating that the nanocomposite effectively initiates this dye's degradation. The results showed that dye degradation was effective even at reduced catalyst concentrations.

1. Introduction

Pursuing green and eco-friendly synthesis methods for advanced materials has become paramount in the contemporary landscape of materials science and environmental sustainability. The urgent need to address environmental degradation and energy challenges has catalyzed the development of novel materials with diverse applications, especially in photocatalysis [1,2]. Composite materials, which combine metal oxides with graphene-based materials, have emerged as promising candidates in photocatalysis [3–5]. These nanocomposites possess a unique interaction, blending the excellent photocatalytic properties of metal oxides with the superior electrical conductivity and high surface area of graphene-based materials. In the case of the CuO-rGO nanocomposite, reduced graphene oxide (rGO) can significantly enhance the copper oxide's charge separation and transport properties (CuO), thereby augmenting its photocatalytic activity. This study's choice of the CuO-rGO nanocomposite is significant due to its versatile photocatalytic properties. Copper oxide (CuO) is a well-known semiconductor material with a narrow bandgap, making it suitable for visible-light-driven photocatalysis [6–9]. The nanocomposite exhibits superior charge separation and catalytic efficiency when combined with reduced graphene oxide (rGO), which provides a conductive and high surface area support structure. This combined effect extends its applicability to various environmental and energy-related photocatalytic processes [10–12].

CuO-rGO nanocomposite offers a wide range of benefits and advantages due to its unique combination of materials. CuO-rGO

* Corresponding author.
E-mail address: satheesphysics@gmail.com (S. Satheeskumar).

https://doi.org/10.1016/j.jics.2024.101423
Received 19 January 2024; Received in revised form 4 October 2024; Accepted 10 October 2024
Available online 18 October 2024
0019-4522/© 2024 Indian Chemical Society. Published by Elsevier B.V. All rights are reserved, including those for text and data mining, AI training, and similar technologies.

nanocomposite has versatile applications in environmental remediation, including removing organic pollutants, heavy metals, and other contaminants from water and air. They can also be employed in energy-related processes, such as hydrogen production through water-splitting reactions. CuO-rGO nanocomposite exhibits significantly improved photocatalytic activity than individual CuO or rGO materials [13–15]. This enhanced activity arises from the synergistic effects of combining a semiconductor (CuO) with a highly conductive and extensive surface area support material (rGO). The presence of rGO facilitates efficient charge separation and transport, increasing photocatalytic efficiency. rGO provides a high surface area, allowing more active chemical reaction sites. This high surface area contributes to the nanocomposite's enhanced catalytic performance, as it can adsorb a greater quantity of reactants and facilitate more reactions. Incorporating rGO into the nanocomposite improves the separation of photogenerated charge carriers (electrons and holes). This reduces the chances of recombination, where electrons and holes combine and neutralize each other, leading to higher photocatalytic efficiency and longer-lasting activity [16–18].

Photocatalysis is an innovative and sustainable process employing semiconductor materials to harness solar or artificial light energy for chemical reactions. It has garnered extensive attention due to its potential applications in addressing critical global issues, including environmental pollution, water purification, and renewable energy generation. Photocatalysts enable the degradation of harmful pollutants and the production of clean energy carriers like hydrogen, making them key players in the transition toward a more sustainable and greener future. Green synthesis methods, also known as sustainable or eco-friendly, are chemical processes used to produce materials, compounds, or nanoparticles while minimizing their environmental impact [19–22]. These methods are designed to reduce or eliminate hazardous chemicals, energy consumption, and waste generation, making them more environmentally friendly and sustainable. Green synthesis methods have gained significant attention in recent years due to their potential to address environmental and health concerns associated with traditional synthesis approaches [23,24].

Eucalyptus leaves, abundant in many regions, present a unique opportunity for green synthesis. *Eucalyptus*-derived compounds are typically biodegradable and environmentally friendly. They contain bioactive compounds that can reduce and stabilize agents during material synthesis. Harnessing the chemical constituents of *Eucalyptus* leaves aligns with sustainability principles and introduces novel elements to the synthesized nanocomposite, potentially enhancing its photocatalytic properties [25–27]. *Eucalyptus* leaves are biogenic precursors for synthesizing the CuO-rGO nanocomposite, exemplifying the commitment to green chemistry principles. *Eucalyptus* leaves contain many bioactive compounds, including essential oils, terpenoids, phenolics, and flavonoids. These compounds have various biological properties, such as antimicrobial, antioxidant, and anti-inflammatory effects, which can be harnessed for diverse applications [28,29]. This approach leverages nature's resources and minimizes the environmental footprint of materials synthesis. *Eucalyptus* leaves are a sustainable source of reducing and stabilizing agents and introduce unique, organic components that may enhance the nanocomposite's performance [30–32].

Here in our study, green synthesized pristine and CuO-rGO nanocomposite was prepared using the hydrothermal method for photocatalytic application using cationic (Rhodamine 6G) and anionic (Rose Bengal) dyes were characterized. Furthermore, their physicochemical properties were also characterized by using X-ray diffraction (XRD), an ultraviolet (UV)–visible spectrophotometer, scanning electron microscopy (SEM) along with energy-dispersive X-ray spectroscopy (EDAX), particle size analysis (PSA), Fourier transform infrared spectroscopy (FTIR). The impacts of copper oxide nanoparticles with reduced graphene oxide (rGO) nanocomposite on the photocatalytic performance using cationic and anionic dyes were scrutinized.

2. Experimental details

The eucalyptus leaves were gathered from villages in the Tamil Nadu region of India. They were washed in deionized water to extract moisture from the gathered leaves. Two days were spent drying the leaves at room temperature after washing. After the leaves had been air-dried and crushed into powder using a household mixer (mixie), 10 g of the milled eucalyptus leaf were dissolved in 250 mL of deionized water and allowed to soak in an Erlenmeyer flask. The mixture was subjected to 70 °C for half an hour. After ensuring that the eucalyptus leaf extract remained undisturbed as it adjusted to room temperature, it was filtered with a sheet of Whatman No.1 filter paper. The finished filtrate was put in storage for further use in other experiments. A sonication-assisted approach was used to create the CuO nanoparticles in an environmentally friendly manner utilizing the leaf extract of eucalyptus leaf. To produce CuO nanoparticles, a precursor solution was generated by combining 2.25 g of copper acetate (0.1 M) precursor (an analytical grade (AR) purchased from Merck, India) to 150 ml of *Eucalyptus* leaf extract and stirring the mixture for 24 h at constant rpm. No further purification of the AR-grade compounds was carried out. Fig. 1 depicts an extraction technique for CuO nanoparticles using *Eucalyptus* leaf extract. The obtained base solution was sonicated for 1 h at 40 kHz till the apparent suspension was observed. After 12 h in a 100 °C hot air oven, the precursor solution, in which the sediments had been suspended, was finally dry. To get the CuO nanoparticles used in subsequent characterization investigations, The dried residue was obtained, subjected to centrifugation at a speed of 5000 rpm, treated to several washes using distilled water and subsequently with ethanol, and finally subjected to calcination at a temperature of 400 °C for 2 h.

A one-pot hydrothermal technique was used to produce the CuO-rGO nanocomposite (also known as CuO-rGO) at a ratio of 10:1. At first, 0.01 g of reduced GO was sonicated for 10 min in a volume of 20 mL ethanol to get a homogeneous dispersion of rGO. After that, the CuO nanoparticles that had been created were dispersed in distilled water (20 mL) for 30 min while being subjected to magnetic stirring to produce a solution that was spread evenly throughout. After that, the rGO dispersion was added to the white suspension prepared and previously agitated for 1 h. After that, the liquid precursor was put into an autoclave lined with Teflon and heated at 160 °C for 16 h. The CuO-rGO nanocomposite was then rinsed and dried at 60 °C for 10 h after the reaction. Then, the dried product is named as CuO-rGO nanocomposite.

3. Photocatalytic activity procedure

A systematic procedure assessed the photocatalytic degradation performance of the CuO and CuO-rGO samples. Initially, a stock solution of dyes was prepared by separately dissolving 10 mg/L of two model dyes, Rhodamine 6G (Rh6G) and Rose Bengal (RB), in distinct beakers. Next, 5 mg/L of the prepared nanocatalyst was added to each dye solution and vigorously stirred without light to ensure a uniform distribution. This step was crucial for facilitating effective interaction between the nanocatalyst and the dye molecules. The subsequent phase involved exposing these prepared solutions to natural sunlight, simulating real-world conditions. During the experiment, absorbance measurements of the Rh6G and RB solutions at their respective maximum absorption wavelengths were taken: 530 nm for Rh6G and 597 nm for RB. To ensure consistent assessment of the photocatalytic degradation kinetics, the reactions were maintained for 120 min. To gain a comprehensive understanding of the degradation process, absorbance readings at regular 15-min intervals throughout the entire 120-min reaction period were recorded.

4. Characterization techniques

The crystallographic analysis of prepared CuO and CuO-rGO samples was analyzed using an X-ray diffractometer (XRD; X'Pert PRO;

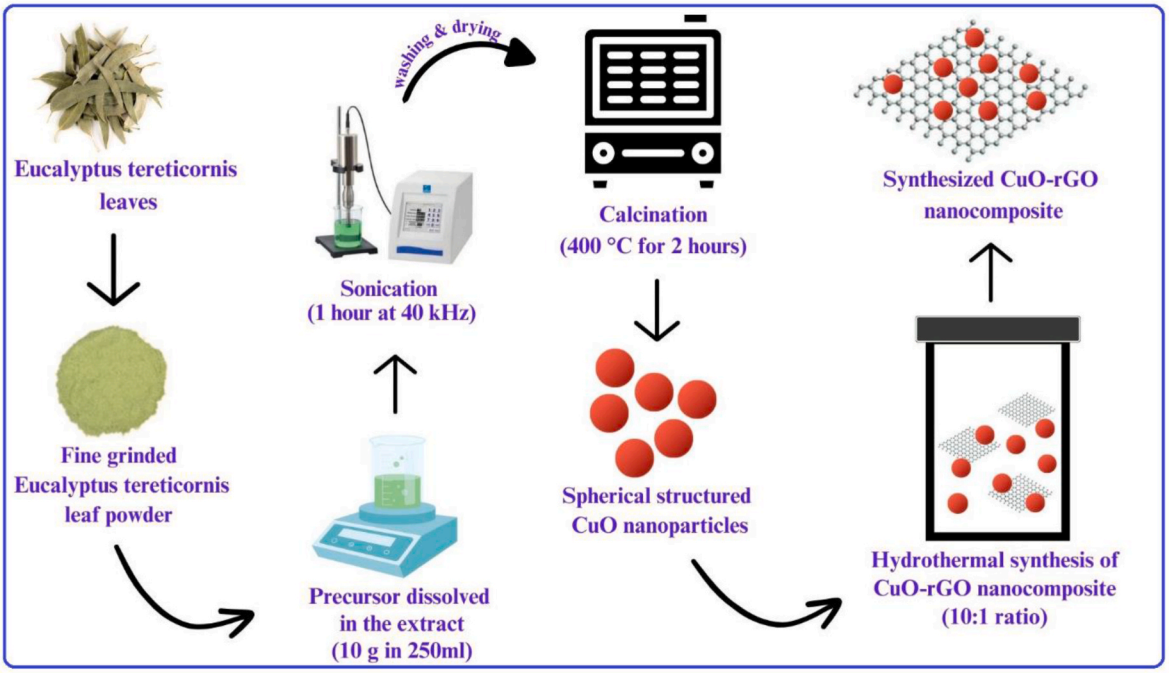


Fig. 1. Synthesis diagram for preparation of CuO-rGO nanocomposite.

PANalytical, the Netherlands). The X-ray diffraction (XRD) analysis employed Cu-Kα radiation with a wavelength of 1.54060 Å as the radiation source, functioning at 30 mA and 40 kV. These samples are scanned at a rate of 10 s per degree (10 s-1) within the angular range of 5–80° (2θ). Subsequently, Rietveld refinement was conducted using the FullProf analytical software to determine the lattice parameters and quantify the agreement among the experimental XRD and standard reference data. At room temperature, Fourier transform infrared spectroscopy (FTIR) using a Spectrum 100 instrument from PerkinElmer, USA, was employed to record the absorption spectrum of the prepared samples in the wavenumber range of 4000 to 400 cm^{-1}. This analysis aimed to investigate the functional groups existing in the samples, and KBr material was used as a background during the FTIR analysis. The particle size analysis of the synthesized samples was conducted through dynamic light scattering via a particle size analyzer (Nanophox, Sympatec, Germany). This analysis was performed at a scattering angle of 90°, covering a size range from 1 to 100 nm. sUV-Vis spectroscopy examined the materials' optical absorbance properties. This spectroscopic analysis used a UV–Vis spectrophotometer (Cary 8454, Agilent Technologies, Singapore), covering a wavelength range of 180–800 nm. Field emission scanning electron microscopy (FESEM) and energy dispersive spectroscopy (EDX) using Bruker's X Flash 7 instrument were employed to examine and characterize the surface features, morphology, and chemical composition. A Thermogravimetric analyzer (TG/DTA - EXSTAR/6300) was exploited to assess the thermal stability of the samples, providing insights into their thermal behavior and decomposition properties. Cationic Rh 6G and anionic RB were employed as model dyes in photocatalytic investigations. The absorbance characteristics of these dyes were monitored at regular 10-min intervals using UV–Vis spectroscopy, carried out with a Cary 8454 spectrophotometer from Agilent Technologies in Singapore. This analysis allowed for the tracking of changes in dye concentration over time, providing valuable insights into the photocatalytic efficiency of the prepared nanocomposite.

5. Results and discussion

5.1. XRD analysis

The XRD pattern in Fig. 2 compares CuO-rGO and CuO with the standard COD card no:96-901-5925 for CuO [33]. The CuO diffraction peaks are sharp and well-defined, indicating high crystallinity. In the CuO-rGO nanocomposite, the major peaks remain similar to pure CuO, suggesting that the crystalline structure of CuO is retained in the nanocomposite. The reduction of graphene oxide does not significantly affect the crystalline nature of CuO. This pattern confirms the successful synthesis of CuO-rGO with retained crystallinity of CuO, consistent with its reported structure. The absence of a distinct rGO peak in the XRD pattern can be attributed to several factors. First, rGO generally has a disordered or amorphous structure due to the reduction process, which removes oxygen-containing functional groups from graphene oxide. This disrupts its crystalline nature, resulting in poorly ordered layers that do not produce sharp diffraction peaks like crystalline materials. Therefore, the typical (002) peak of graphene oxide, usually observed around 24–26°, is either very weak or absent in rGO due to the lack of

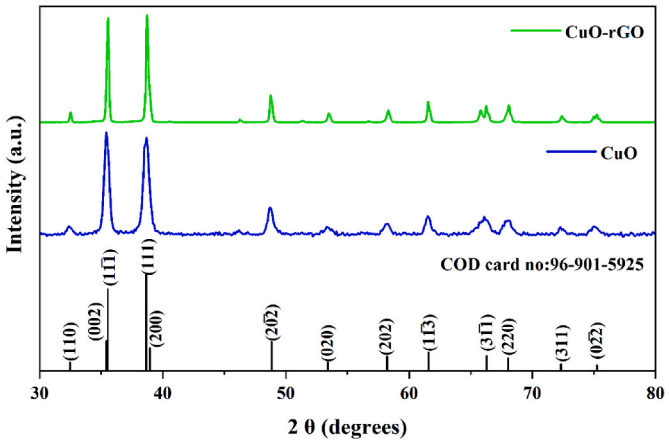


Fig. 2. XRD analysis of prepared CuO and CuO-rGO nanocomposite.

interlayer ordering [34].

On the other hand, the quantity of rGO in the CuO-rGO nanocomposite might be relatively low, making its signal hard to detect compared to the much more crystalline and intense CuO peaks. The CuO NPs phase, being more crystalline, dominates the diffraction pattern, and the weaker rGO signal could be masked or overshadowed. However, the presence of GO peaks is evident in refinement; additionally, the elemental presence was further evaluated with EDAX analysis. The average crystalline size of the synthesized samples was calculated using the Debye-Scherrer equation. As outlined in Table 1, the prepared CuO average crystalline size is approximately 13.7 nm, while the CuO-rGO nanocomposite exhibits a considerably smaller crystalline size of approximately 20.2 nm. The other structural parameters calculated from the XRD patterns are shown in Table 1. During the synthesis, rGO sheets provide a platform where CuO NPs can nucleate and grow more uniformly. The presence of rGO reduces the agglomeration of CuO NPs, promoting more controlled and homogeneous crystal growth, which can lead to larger crystallite sizes. The observed increase in crystalline size for CuO NPs in the CuO-rGO nanocomposite can be attributed to the role of rGO in supporting and controlling the crystal growth process, preventing particle aggregation, and reducing grain boundary formation, all of which contribute to the development of larger CuO crystallites.

Moreover, Rietveld refinement was conducted to evaluate the correspondence between the calculated and observed XRD patterns. The refinement process involved adjusting various parameters, including background, peak shape, atom positions, scale factors, and lattice functions. Fig. 3 illustrates the alignment between the observed and calculated data for CuO and CuO-rGO nanocomposite samples. This analysis demonstrates that the inclusion of rGO has minimal impact on the crystal structure, affirming the structural stability of the CuO NPs. Additionally, the refinement parameters, including Rp, Rwp, Rexp, and Chi^2 values (as presented in Table 1), confirm the absence of additional impurities in the prepared samples and indicate a good fit with the calculated XRD patterns. These refinement results are reliable compared to previous findings, and they corroborate the structural integrity of the synthesized materials without significant alterations due to the incorporation of rGO [35,36].

5.2. FT-IR analysis

Fourier Transform Infrared spectroscopy is a method for measuring the vibrational frequencies of a molecule's bonds. The FTIR spectra of CuO nanoparticles and CuO-rGO are revealed in Fig. 4. A broad absorption peak at 3471 cm^{-1}, corresponding to the stretching vibration of O–H bonds, suggests the possible presence of adsorbed water molecules and carboxy and hydroxy O–H groups. A peak at 1634 cm^{-1}, attributed to the stretching of C=C bonds, indicates the presence of a graphene nanosheet. Also, two distinct peaks at 2921 and 2851 cm^{-1} suggest that the carbon basal planes in rGO have been well-maintained. The observed peaks at a wavenumber of 1385 cm^{-1} may be attributed to the bending behavior of the C–OH functional group [37,38].

In the case of CuO-rGO, the peak levels for oxygen-containing function groups become higher. The characteristic vibration peaks around 841 cm^{-1} are assigned to the stretching mode of the Cu=O. This phenomenon may be explained in the following manner. During photoreduction, copper ions are reduced on the surface of rGO. This reduction reaction leads to the generation of holes inside the rGO material. These photogenerated holes can oxidize the rGO, enhancing oxygen-containing functional groups on the rGO surface. The band seen at a wavenumber of 1634 cm^{-1} corresponds to the aromatic C=C functional group, which may be ascribed to the existence of Sp^2 hybridized carbon atoms forming rings with graphitic features [39–41].

5.3. UV–visible spectroscopy

The optical properties of CuO and CuO-rGO samples were investigated using UV–vis spectra, as mentioned in Fig. 5. The UV–Vis absorbance peaks for CuO and the CuO-rGO nanocomposite were detected at 233 nm and 230 nm, respectively. The observed transitions in the CuO-rGO nanocomposites may be attributed to n–π* and π–π* interactions arising from aromatic carbon-carbon bonds and carbonyl groups [42]. The absorbance spectrum demonstrates the decrease in graphene oxide (GO) and the corresponding replacement of the hydroxyl (OH) and carboxyl (COOH) groups with copper oxide [43]. The observed transition may be attributed to the adhesion of CuO nanoparticles onto the surface of rGO sheets. The spectrum shows a blue shift, indicating the formation of the nanocomposite. This shift might be attributed to the sticking of CuO nanoparticles on the surface of rGO sheets. The surface plasmon resonance effect of CuO nanoparticles provided UV–visible absorption spectra of rGO displayed with them additional peaks at 640 nm. The peak's morphology and spatial orientation depend upon the diameter of the copper nanoparticle. This proves that Cu nanoparticles were successfully deposited onto the rGO surface.

The determination of the bandgap of the prepared CuO nanoparticles and the nanocomposite was accomplished via the Tauc plot equation.

$$(\alpha h\nu)^n = E(h\nu - E_g)$$

α represents the absorption coefficient, hv symbolizes photon energy, E stands for a constant, Eg denotes the optical bandgap energy, and n signifies the Tauc exponent. The Tauc exponent's value relies on the type of optical transition; for direct transitions, n is typically equal to 1/2, while for indirect transitions, it is approximately equal to 2. The bandgap energy value may be determined by plotting the $(\alpha h\nu)^2$ against the incoming photon energy ($h\nu$) and extrapolating the linear segment of the curve to zero absorption coefficient. The corresponding bandgap energies for CuO NPs and CuO-rGO nanocomposites are determined to be 2.19 eV and 2.79 eV, respectively. The observed blue shift in the bandgap energy may be assigned to the quantum confinement effect due to a reduction in particle size [44].

5.4. Thermal analysis

TGA was conducted to inspect the thermal stability of the prepared pure CuO nanoparticles and the CuO-rGO nanocomposite. These results, highlighted in Fig. 6, provide significant insights into the response and behavior of the materials as temperatures increase. In the case of the CuO nanoparticles, the TGA analysis revealed a total weight loss of approximately 6.30 %. The observed increase in the total weight of the samples, around 250 °C, is associated with the process of copper oxidation. Conversely, the TGA analysis of the CuO-rGO nanocomposite displayed a significantly reduced weight loss of approximately 10 %.

Moreover, embedding rGO nanosheets will enhance the heat transfer

Table 1
XRD and Rietveld parameters for CuO and CuO-rGO nanocomposite.

Sample	Average crystalline size (nm)	Dislocation density (δ) (× 10^{15} lines/m^2)	Micro strain (%)	Lattice parameters (Å)	Cell volume (Å)	Rietveld agreement indices			
						R_p	R_{wp}	R_{exp}	χ^2
CuO	13.7	5.3	0.133	a = 4.67, b = 3.42 & c = 5.13	81.09	5.25	6.8	4.8	1.95
CuO-rGO	20.2	2.4	0.125	a = 4.68, b = 3.42 & c = 5.12	81.19	6.3	5.04	3.91	1.98

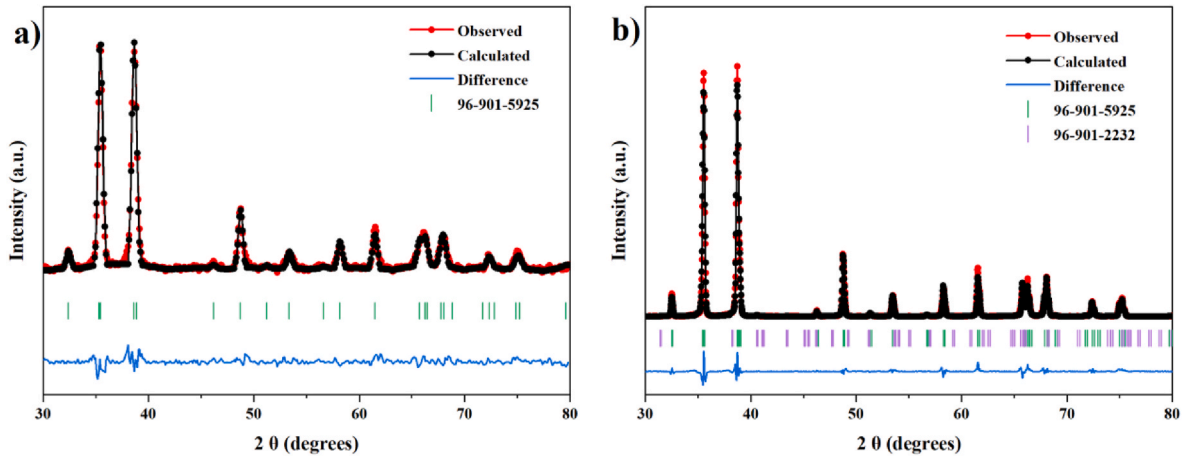


Fig. 3. Rietveld Refinement fitting of a) CuO NPs and b) CuO-rGO nanocomposite.

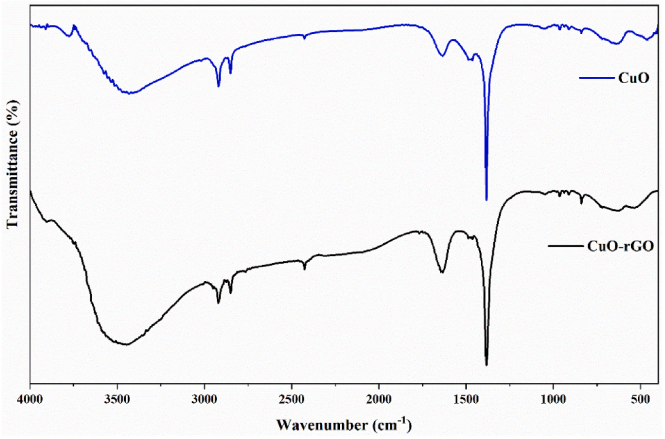


Fig. 4. FT-IR spectra of prepared nanocomposite.

path. However, the initial weight loss of pure CuO is comparatively higher than that of the CuO-rGO nanocomposite. The thermal stability of rGO sheets provides a protective barrier for the underlying CuO nanoparticles, preventing their thermal breakdown until high temperatures are attained. The thermal degradation curve showed clear and distinct stages.

At lower temperatures, an initial decrease in weight of 4.7 % was recorded. The primary cause of this initial decrease may be the elimination of physically adsorbed water and other volatile substances on the nanoparticles' surface. Following this, a significant reduction in weight of 5.3 % was observed within the temperature range associated with the breakdown of organic residues and the probable presence of surfactants or capping agents added during the synthesis procedure. Above 250 °C–910 °C, it has the weight loss that is due to carbon group compounds. Above the 600 °C weight loss may be due to oxygen loss. This enhanced thermal stability implies that the prepared materials retain activity over extended periods and in varying temperatures when used as catalysts. This aspect is crucial for sustaining efficient and effective photocatalytic processes.

5.5. *Particle size and zeta potential analysis*

The average particle size was determined using a particle size analyzer that used dynamic light scattering as its operating phenomena, using a laser input intensity of 532 nm. Fig. 7 (a) displays the particle size distribution of prepared CuO nanoparticle and CuO-rGO nanocomposite.

The particle size analysis of the CuO nanoparticles revealed a distribution ranging from approximately 4 nm (d_{10}) to 80 nm (d_{90}), with an average particle size of 30.15 nm (d_{50}). In comparison, the CuO-rGO nanocomposite exhibited a smaller mean particle size of 20.2 nm (d_{50}), with the particle size distribution extending from around 3 nm

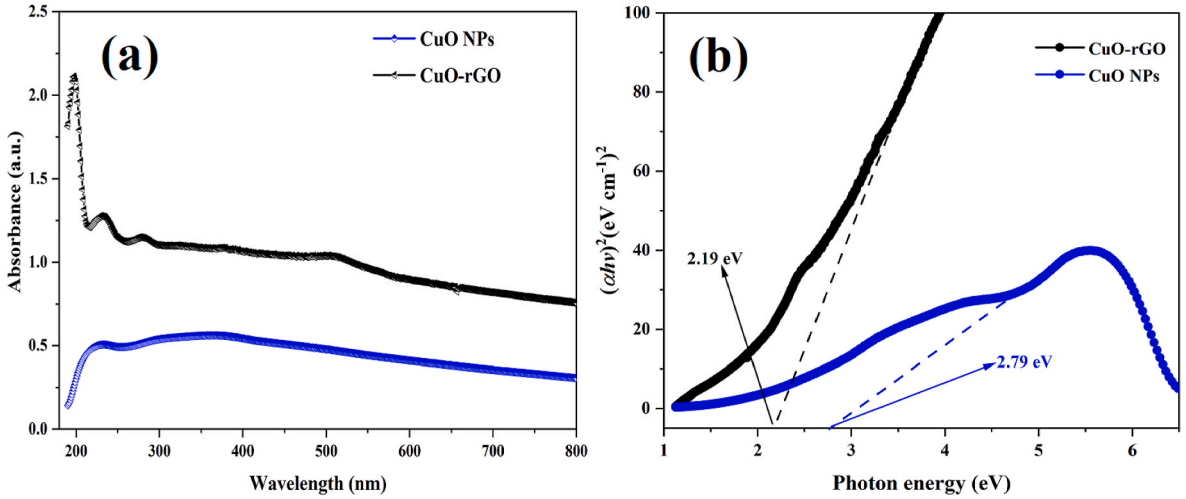


Fig. 5. UV–Vis spectra of prepared CuO nanoparticles and CuO-rGO nanocomposite.

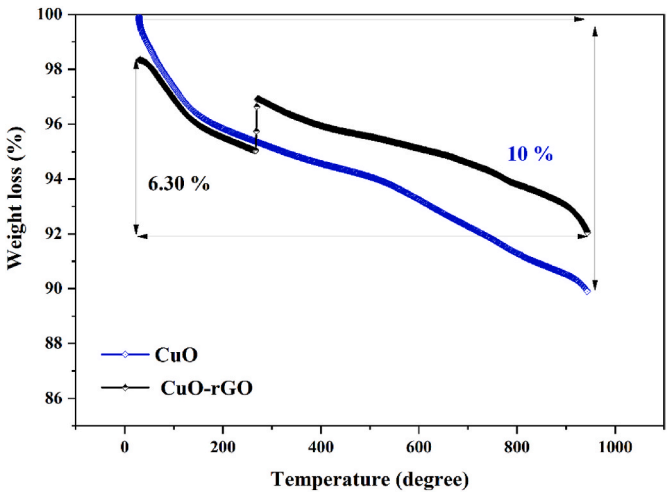


Fig. 6. Thermogravimetric analysis of prepared nanocomposite.

(d_{10}) to 160 nm (d_{90}). The reduction in particle size within the nanocomposite, relative to the pure CuO nanoparticles, can be attributed to the uniform dispersion of the CuO nanoparticles within the rGO matrix [45]. The hydrothermal synthesis method, employed for composite preparation, plays a crucial role in achieving this uniform dispersion. The process effectively prevents nanoparticle agglomeration and promotes controlled growth, leading to a more consistent distribution of smaller particles throughout the rGO sheets. As a result, the nanocomposite demonstrates a finer particle size distribution than the pure CuO nanoparticles, further enhancing its potential for applications requiring a high surface area and improved reactivity.

The surface charge and colloidal stability of the CuO nanoparticles and the CuO-rGO nanocomposite were evaluated by zeta potential measurements. The findings, as shown in Fig. 7(b and c), provide significant insight into the electrostatic characteristics of these materials. Significantly, the zeta potential findings exhibited unique values for the two compounds. The zeta potential of the CuO nanoparticles was measured to be −9.0 mV. In contrast, the CuO-rGO nanocomposite exhibited a significantly greater negative zeta potential of −58.9 mV. The observed significant decrease in the zeta potential of the CuO-rGO nanocomposite may be attributed to including rGO. The negative charge of reduced graphene oxide is attributed chiefly to the presence of oxygen-containing functional groups. The rGO results in a significantly enhanced negative zeta potential in the nanocomposite material. The observed variation in zeta potential values highlights the significant impact of rGO on the surface charge of the nanocomposite material. The CuO-rGO nanocomposite has a significantly negative zeta potential, which might have important consequences for its colloidal stability and interactions with other particles or molecules in broad catalytic applications.

5.6. FE-SEM and EDAX analysis

As depicted in Fig. 8(a), the FESEM image of the synthesized CuO nanoparticles reveals a distinctive foam-like morphology characterized by clustered and porous structures. This unique morphology can be attributed to the sonication-assisted synthesis, combined with the effective role of *Eucalyptus* leaf extract as a reducing and stabilizing agent. The use of this extract in the synthesis process has been shown to enhance the formation of well-defined CuO nanoparticles, promoting a

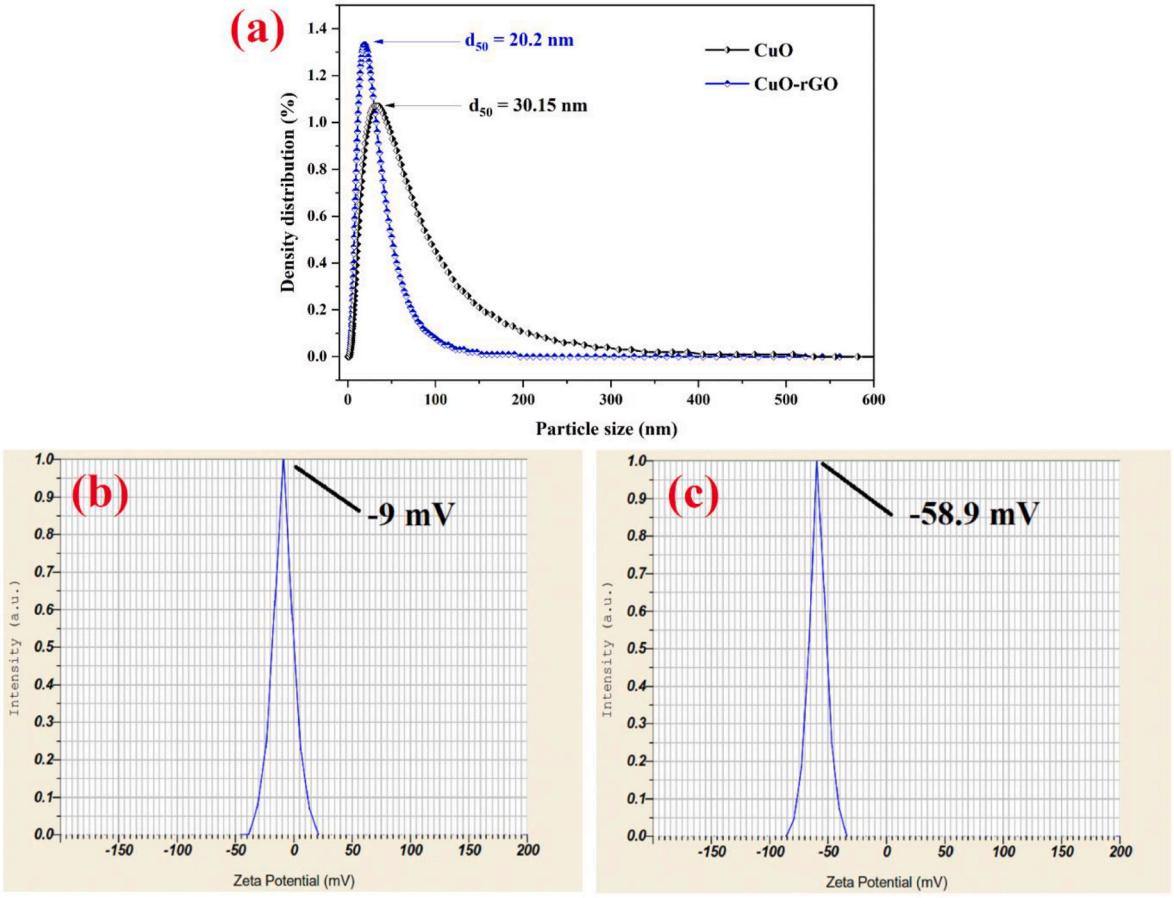


Fig. 7. (a) Particle Size analysis, (b and c) Zeta potential of prepared CuO nanoparticles and CuO-rGO nanocomposite.

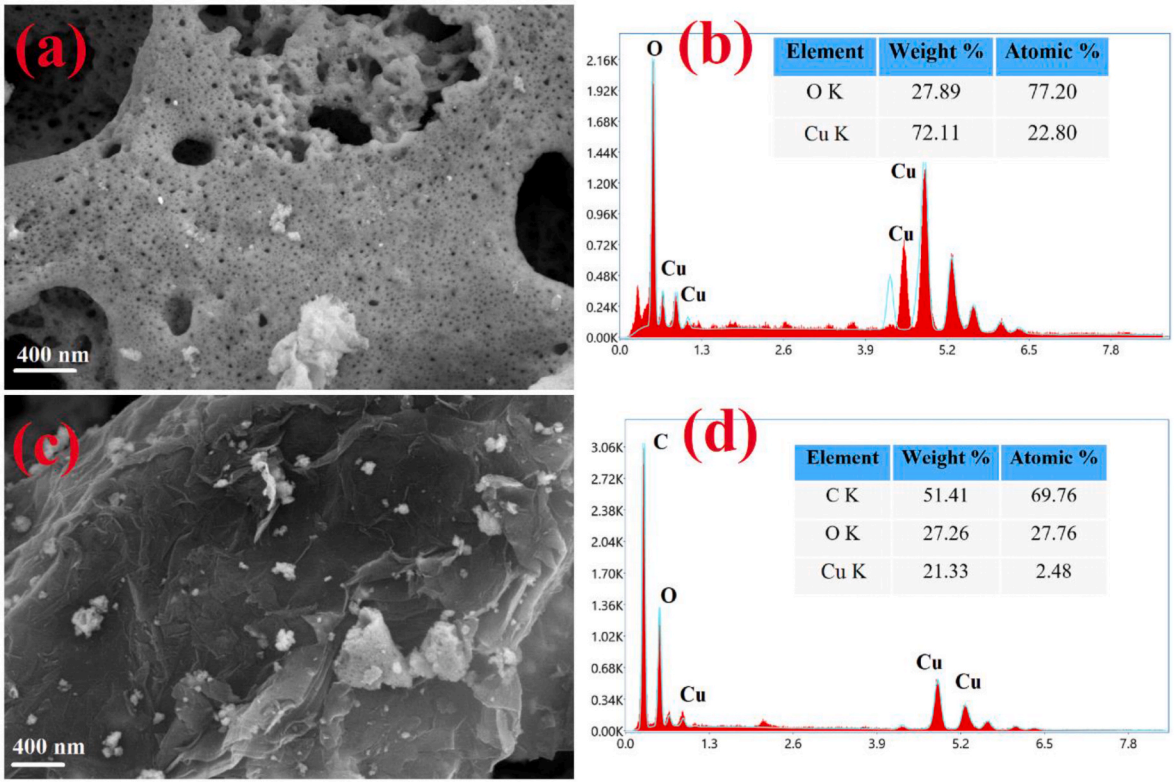


Fig. 8. FESEM image of a) CuO and c) CuO-rGO nanocomposite and elemental analysis of b) CuO and d) CuO-rGO.

controlled nucleation and growth process. Fig. 8(c) illustrates the FESEM micrograph of the CuO-rGO nanocomposite, where the CuO nanoparticles are uniformly dispersed as nanospheres throughout the rGO matrix. The rGO sheets exhibit a porous, sponge-like morphology, characterized by rippling, crumpling, and a randomly arranged structure, yet maintaining an interconnected layered architecture. The uniform distribution of spherical CuO nanoparticles within the rGO matrix is facilitated by the synergistic reduction and stabilization capabilities of *Eucalyptus* extract during the sonication-assisted approach. The CuO-rGO nanocomposite exhibits a minimal aggregation, ensuring a homogeneously distributed nanostructure. The CuO particles, formed at the nanoscale, display enhanced surface reactivity due to their small size, as supported by the XRD analysis, which confirms the presence of Cu^{2+} species. This transformation, driven by hydrothermal treatment conditions, is critical for catalytic and photocatalytic applications, where the higher valence state of Cu enhances the material's overall reactivity.

Additionally, nano-porous copper led to the formation of uniformly distributed tiny CuO nanoparticles on well-dispersed rGO nanosheet. The rGO nanosheets demonstrate a significant graphitization level and a decrease in oxygen-containing functional groups. This specific structural characteristic improves the capacity of the material to provide support and stability to CuO nanoparticles. This, in turn, promotes the effective transfer of charges and facilitates combined effects in photocatalytic applications. The elemental composition of the synthesized CuO and CuO-rGO nanocomposite was confirmed through EDAX analysis, shown in Fig. 8 (b and d), providing detailed insights into its chemical structure. The analysis verified the presence of key constituents, primarily Copper (Cu), Oxygen (O), and Carbon (C), with their respective energy peaks observed at high intensities. As shown in Fig. 8(b), the prominent signals for Cu and O confirm the formation of CuO nanoparticles within the composite. This is consistent with the expected stoichiometry of copper oxide and reflects the successful synthesis of CuO in the nanocomposite. In addition, the detection of Carbon in the EDAX spectrum indicates the presence of rGO nanosheets, confirming their successful incorporation into the composite material. The inclusion of rGO contributes to the overall structure and functionality of the nanocomposite, enhancing properties such as electrical conductivity and surface area.

5.7. Photocatalytic dye degradation activity

The bonding of CuO nanoparticles and CuO/rGO nanocomposite has enhanced significant properties, including decreased recombination of charges (electrons and holes) and improved absorption of visible light. These qualities are essential for the development of an effective photocatalyst. The photocatalytic performance of CuO nanoparticles and CuO/rGO nanocomposite was assessed by observing the different cationic (Rhodamine 6G) and anionic (Rose Bengal) dyes over time under the influence of light irradiation, using UV–visible spectroscopy. The dye has a prominent absorption peak at wavelengths of 530 nm for cationic rhodamine 6G dye and 550 nm for anionic Rose Bengal dye, and the absorbance of the dye at its initial concentration was measured. The decrease in absorbance of the dye was seen as the duration of light irradiation increased, as shown in Fig. 9. The decrease in absorbance observed presents strong evidence for the efficient degradation of the dyes aided by the created samples when exposed to visible-light irradiation. The following equation was used to derive the prepared samples' photocatalytic degradation efficiency:

$$\text{Dye Degradation efficiency} = \frac{(D_0 - D_t)}{D_0}\ \%$$

D_0 denotes the initial concentration of the dye solution, and D_t signifies the dye concentration at time t.

Using the above mentioned equation, the photodegrading efficiency of CuO nanoparticles towards RB and Rh6G within 120 min was determined to be 90.79 % and 91.37 %, respectively. In the same way, the degrading efficiency of the CuO-rGO nanocomposite is found to be 91.47 % for RB and 96.48 % for Rh6G in Fig. 10. Distinctly, the degrading efficiency of the CuO-rGO nanocomposite is greater than that

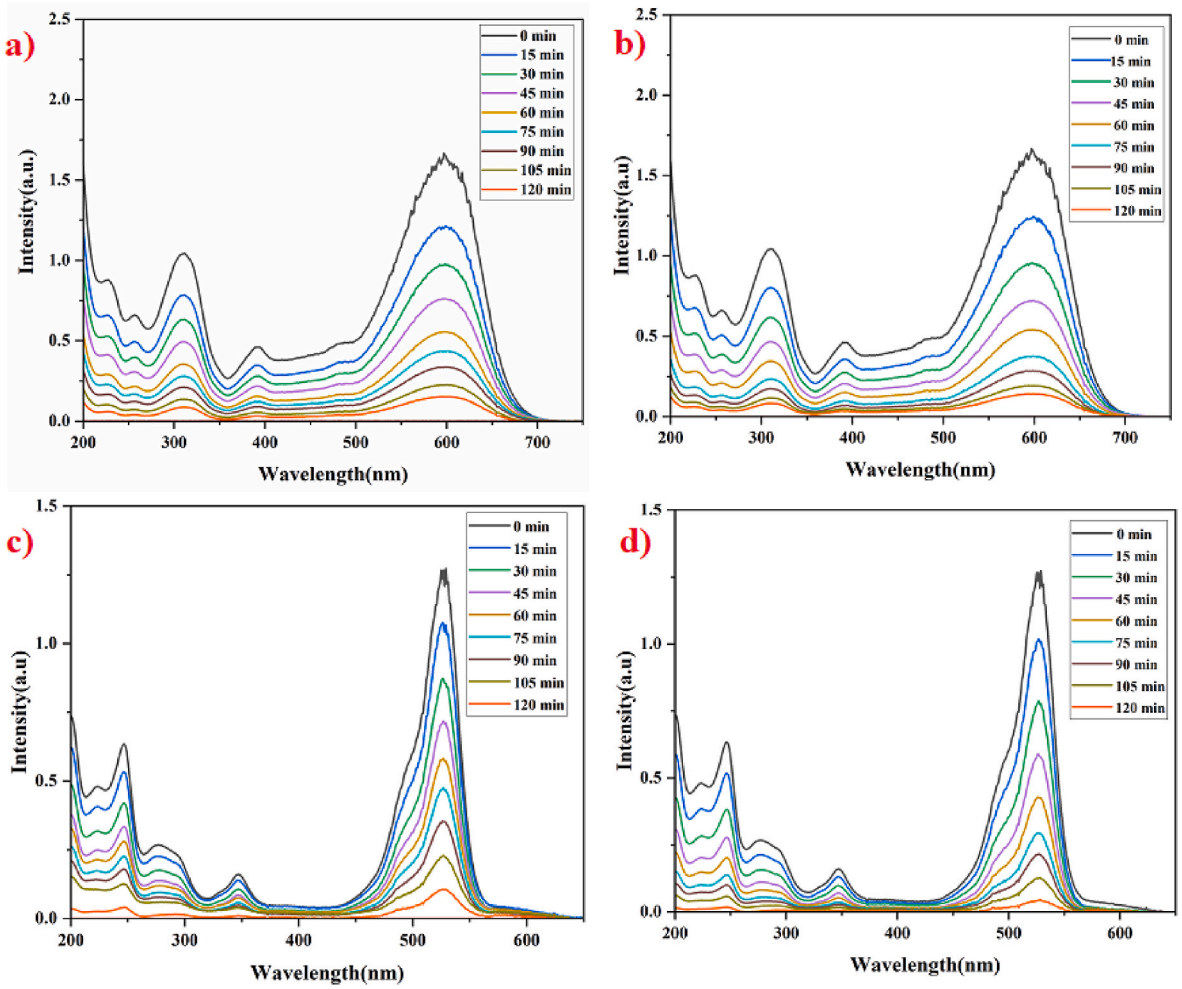


Fig. 9. Absorbance-dye degradation graph of Rose Bengal a) CuO, b) CuO-rGO and Rhodamine 6G c) CuO, d) CuO-rGO.

of pure CuO nanoparticles. Photocatalytic degradation efficiency is summarized in Table 2. The improvement in photocatalytic performance may be ascribed to different factors. The CuO-rGO nanocomposite is characterized by a reduced optical band gap, which enhances its efficiency in absorbing visible light for photocatalytic processes (see Fig. 11).

Furthermore, integrating rGO offers an increased concentration of sites for interaction between dyes and nanoparticles, enhancing the degradation mechanism. Moreover, the significant increase in the degradation efficiency for Rh6G dye indicates the formation of π–π conjugation and electrostatic interactions [46]. The observed interactions occurred due to the parallel alignment of electron-rich π orbitals in the rGO nanosheets and the aromatic rings found in the Rh6G dye molecules. Moreover, the presence of a negative charge on the surface of the created nanocomposite enhances the binding of cationic dyes, hence enhancing the effectiveness of degradation.

The primary light absorber in this instance is the rGO, and separating the photogenerated electrons and holes is notably efficient when copper nanoparticles are present. Moreover, the exceptional photocatalytic efficacy shown by the CuO/rGO nanocomposite may be attributed to the catalytic influence imposed by the presence of copper. The CuO nanoparticle has favorable characteristics as a photoelectron acceptor, effectively capturing photoelectrons and reducing the recombination rate of photoelectron-hole pairs. This process facilitates an effective transfer of charge carriers to the surface of rGO for dye degradation. Subsequently, the photoelectron has the potential to be involved in a reaction with the oxygen molecules present in the solution, resulting in the formation of Superoxides capable of oxidizing the dye.

The degradation kinetics of the prepared samples were assessed utilizing a first-order kinetic model.

$$ln\left(\frac{C}{C_0}\right) = -kt$$

In this equation, C and C_0 denote the concentration at a specific time and the initial concentration of the dye, respectively, while k represents the rate constant of the reaction.

Fig. 10(a and b) displays the C/C_0 curve, which represents the changes in concentration noticed in the absence of a catalyst and the presence of dye solutions loaded with nanocatalysis. This graph illustrates the progressive reduction in dye molecules over time (120 min). As described by Fig. 10(c and d) and tabulated in Table 1, the calculated kinetic parameters for the synthesized CuO nanoparticles with the degradation of RB and Rh6G dyes are 1.84×10^{-2} and 1.92×10^{-2} min^{-1}, respectively. Similarly, the kinetic values for the created CuO-rGO nanocomposite are 2.05×10^{-2} and 2.55×10^{-2} min^{-1}, respectively. The CuO-rGO nanocomposite has a significantly higher degradation rate than CuO nanoparticles, with an estimated increase of 1.4 times. The increased degradation rate may be attributed to the reduced bandgap rGO offers. The reduction in the band gap of CuO effectively reduces the recombination of electron-hole pairs, leading to increased absorption of photons for excitation and charge separation. Efficient electron transfer between CuO and dye molecules may explain why CuO-rGO is more effective than CuO nanoparticles in photocatalytic dye degradation. The transmission of electrons from the conjugated

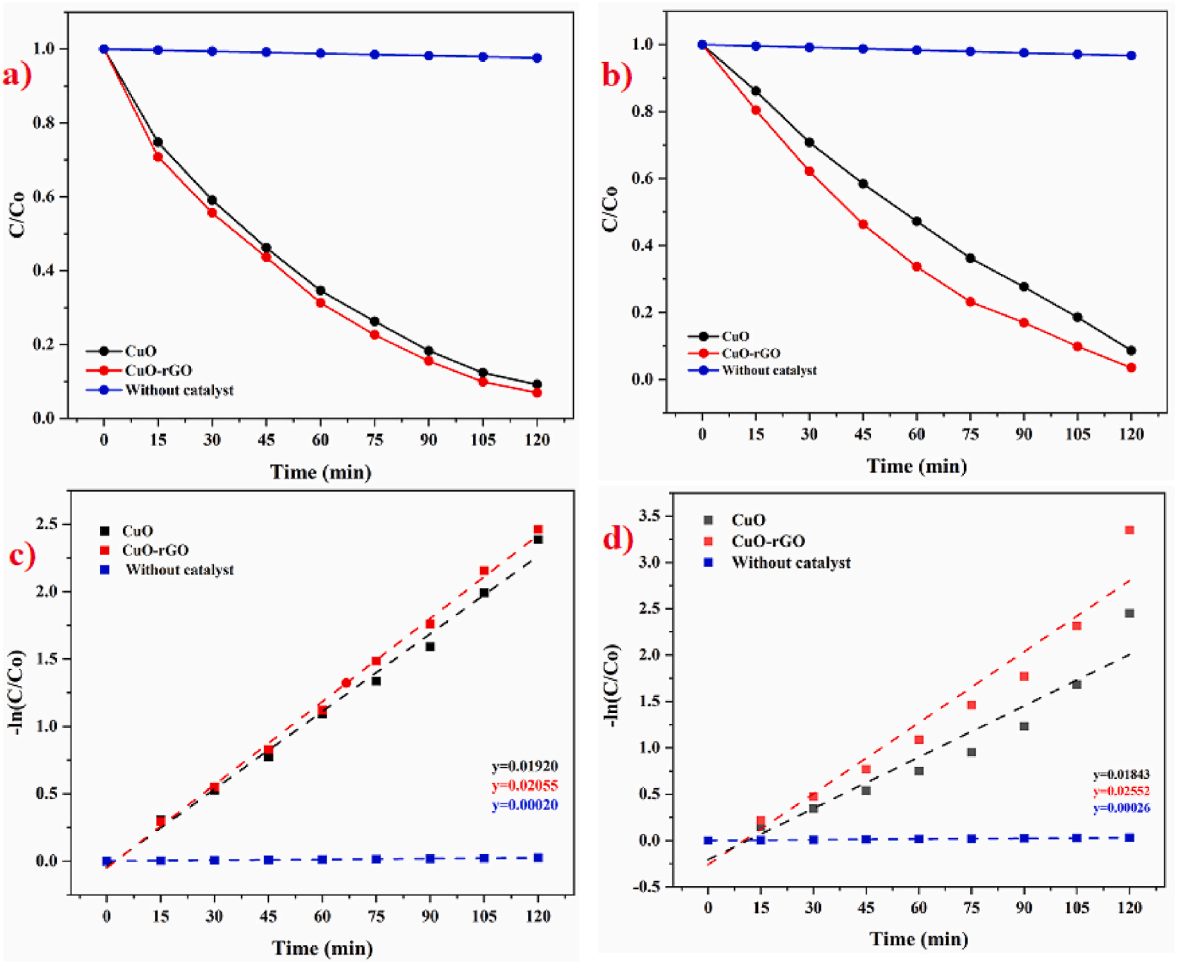


Fig. 10. C/C_0 curves for Rose Bengal (a) and Rhodamine 6G (b), along with pseudo-first-order degradation kinetics for Rose Bengal (c) and Rhodamine 6G (d).

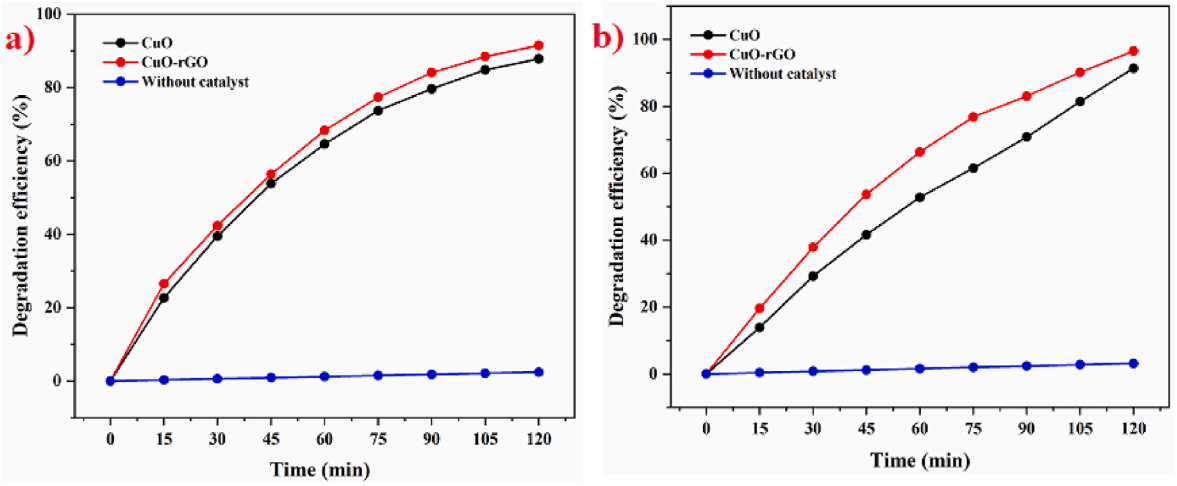


Fig. 11. CuO nanoparticle and CuO-rGO degradation efficiencies against a Rose Bengal (a) and Rhodamine 6G (b) dyes.

graphene to the adsorbed dye molecules induces a redox breakdown. As summarized in Table 3, previous research endeavors have employed a variety of model dyes as test compounds in their investigations, often incorporating various metal oxide nanomaterials with reduced graphene oxides to enhance photocatalytic performance.

5.8. Dye degradation mechanism

Hence, the photoactivity of the CuO nanoparticles and CuO-rGO nanocomposites is seen in the degradation process of Rh6G and RB dyes. The degradation of dyes by photocatalysis may be achieved through direct or indirect mechanisms. Decomposition occurs in the direct route, following the photosensitization of dyes through photon

Table 2
Photocatalyst with dye degradation rate constant and its efficiency for 120 min visible light irradiation.

Photocatalyst	Dye	Concentration of dye (mg/L)	Photocatalyst Concentration (mg)	Kinetic rate constant (x 10^{-2} min^{-1})	Degradation efficiency (%)
CuO	RB	10	5	1.84	90.79
	Rh6G			1.92	91.37
CuO-rGO	RB	10	5	2.05	91.47
	Rh6G			2.55	96.48

Table 3
Comparative photocatalytic degradation of dyes with previous reports and this study.

Catalyst	Synthesis method	Dye used	Catalyst concentration (mg/L)	Dye concentration	Irradiation source	Irradiation time	Degradation efficiency (%)	Ref
g-C_3N_4/rGO/SnO_2	Chemical	Rhodamine B	30	7	Visible light	120	83.2	[54]
SnO_2–Fe_2O_3-rGO	Chemical	Methylene Blue	50	10	Sunlight	180	78.4	[55]
SnO_2	Green	Eriochrome Black T	~210	6	Visible light	270	77	[56]
SnO_2–ZnO	Green	Eriochrome Black T	15	100	Sunlight	180	98	[57]
SnO_2-WO_3	Green	Methylene Blue	20	5	Visible light	180	75	[58]
La_2FeO_3-rGO-NiO	Chemical route	Congo red	50	50	Visible light	90	96	[59]
$BiFeO_3$–CdS-rGO	Chemical route	Methyl orange	70	20	Visible light	90	89	[60]
CuO	Green route	Rose Bengal	5	10	Sunlight	120	90.79	Present
CuO	Green route	Rhodamine 6G	5	10	Sunlight	120	91.37	work
CuO-rGO	Green route	Rose Bengal	5	10	Sunlight	120	91.47	
CuO-rGO	Green route	Rhodamine 6G	5	10	Sunlight	120	96.48	

absorption. This process is followed by the insertion of photoexcited electrons into the conduction band of the semiconductor catalyst. As a result, dissolved oxygen is reduced to form superoxide radical ions (O_2-•), which further react to form highly reactive hydroxyl radicals (•OH). The two radicals mentioned above are primarily responsible for initiating the degradation processes.

Decomposition through the indirect process of the in-situ creation of electron-hole pairs. When semiconductor catalyst particles are exposed to radiation with an energy level of (hν), it has been observed that the energy of the radiation (hν) is equal to or greater than the band gap energy (Eg) of the particles. Subsequently, the conduction band (CB) electrons reduce electron-accepting species, such as dissolved O_2 in the solution, leading to the formation of O_2-• ions. On the other hand, the valence band (VB) holes facilitate the oxidation of electron-donating species, such as H_2O, resulting in the generation of •OH radicals [47]. Subsequently, the breakdown begins with intermediate products, finally into environmentally harmless substances such as carbon dioxide (CO_2), water (H_2O), and a small number of mineral acids [48]. Among the two possible methods for decomposition, it has been shown that the indirect approach exhibits incredible kinetic speed and serves as the primary route for the breakdown of organic contaminants. The following equations provide insight into the possible mechanism for dye degradation by the prepared CuO and CuO-rGO nanocomposite:

$$rGO - CuO + h\nu \rightarrow rGO - CuO\ (e - + h +)$$

$$\mathbf{h^+ + H_2O \rightarrow H^+ + OH^-}$$

$$\mathbf{e^- + O_2 \rightarrow O_2^-}$$

$$\mathbf{O_2^- + H^+ \rightarrow HO_2}$$

$$RB + Rh6G + {}^{*}HO + O2 - \rightarrow \text{Degraded products } (CO_2 + \mathbf{H_2O})$$

The probable photocatalytic degradation process of the synthesized samples is indicated in Fig. 12. CuO and the CuO-rGO nanocomposite undergo an intense photocatalytic degradation process that involves photon absorption. They participate in numerous methods, such as hydroxylation, dehydrogenation, and the oxidative cleavage of dye functional groups, breaking dye molecules into smaller and less complicated byproducts [49]. Concurrently, dye molecules are adsorbed onto the catalyst's surface via physical interactions, enhancing the proximity to the active sites [50]. The photocatalytic process continues with the constant regeneration of photogenerated charge carriers as they absorb more photons, allowing the catalyst to maintain its catalytic activity. In the case of the CuO-rGO nanocomposite, reduced graphene oxide sheets play a vital role in enabling electron transfer, enhancing charge separation and transport efficiency. Additionally, rGO offers an extra surface area for dye adsorption, significantly increasing the photocatalytic efficacy [51].

Electrons can undergo transfer to the surface of nanoparticles, subsequently leading to their movement toward graphene [52]. Therefore, the recombination rate of electron-hole pairs might decrease as the size of the nanoparticles decreases. The photocatalytic activity was enhanced due to the transfer of electrons from graphene to dye molecules. The improved catalytic performance of CuO-rGO nanocomposites in the degradation of dye can be primarily attributed to the combined

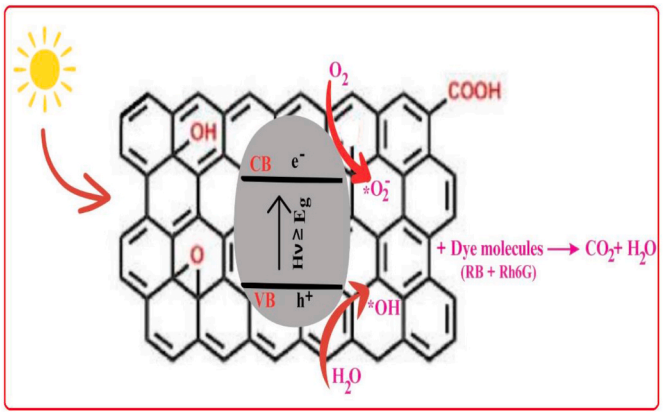


Fig. 12. Degradation mechanism for prepared CuO-rGO nanocomposite.

effect of the high absorptivity of dye molecules on rGO, the presence of surface hydroxyl groups that facilitate the generation of hydroxyl radicals (•OH), and the advantageous photocatalytic properties of CuO nanoparticles, including a lower bandgap and smaller particle size [53].

5.9. Cyclic stability

The cyclic stability of the synthesized CuO and CuO-rGO nanocomposites was evaluated over five consecutive cycles by collecting the photocatalyst after each run and washing it with 70 % ethanol, followed by centrifugation. As shown in Fig. 13, the concentration profiles of RB and Rh6G model pollutants gradually decreased even after the fifth cycle, indicating sustained photocatalytic degradation. Furthermore, the degradation efficiency of the CuO nanoparticles dropped by 12.13 % and 8.27 % for RB and Rh6G after five cycles, likely due to the accumulation of dye molecules on the active sites, which hinders further degradation. In contrast, the CuO-rGO nanocomposite exhibited a significantly smaller decrease in degradation efficiency, with only 3.6 % and 3.15 % for RB and Rh6G pollutants. This improved cyclic stability is attributed to the role of rGO as a supporting matrix, effectively dispersing the metal oxide nanoparticles across its surface. This dispersion prevents nanoparticle agglomeration, preserving the high surface area and catalytic activity over multiple cycles. Additionally, rGO enhances electron mobility by acting as a conductive pathway, facilitating rapid electron transfer from the excited CuO nanoparticles and reducing electron-hole recombination. As a result, the CuO-rGO nanocomposite maintains superior photocatalytic performance over repeated cycles, demonstrating its robustness as a photocatalyst compared to pure CuO nanoparticles.

6. Conclusion

Using *Eucalyptus tereticornis* as a stabilizing and reducing agent during the synthesis of CuO nanoparticles resulted in a high degree of crystallinity. A simple hydrothermal approach effectively incorporated these nanoparticles with rGO. Integrating rGO during the nucleation stage of CuO nanoparticles has significantly enhanced several combination factors, including optical characteristics, thermal performance, crystalline structure, particle sizes, zeta potential, and morphology. XRD investigation validated the monoclinic phase composition and crystallinity of CuO and CuO-rGO nanosheets. The particle size was carried out via the Scherrer equation. The Cu-rGO sheets exhibit enhanced optical absorbance characteristics and demonstrate high efficiency in minimizing the recombination of charge carriers. The results obtained from TGA and FTIR analysis confirmed the removal of oxygen-containing functional groups. In addition, the use of CuO-rGO samples was shown to be significant in the degradation of RB and Rh6G dyes, achieving a maximum degradation efficiency of 91.3 % and 96.4 %, respectively, within a 120-min duration, when exposed to visible light in an aqueous solution. The observed phenomenon may be attributed to the significant surface area of the sheets and a decreased probability of charge-carrier recombination. The rate constant for the photodegradation of Rh6G dye in the presence of CuO and Cu-rGO samples was determined to be 1.92 and 2.55 X10^{-2} min^{-1}, respectively. The prominent impact of adding rGO to CuO has been evidenced in cyclic stability, creating a robust nano photocatalyst.

CRediT authorship contribution statement

S. Satheeskumar: Data curation, Formal analysis, Funding acquisition, Supervision, Writing – original draft. **S. Surendhiran:**

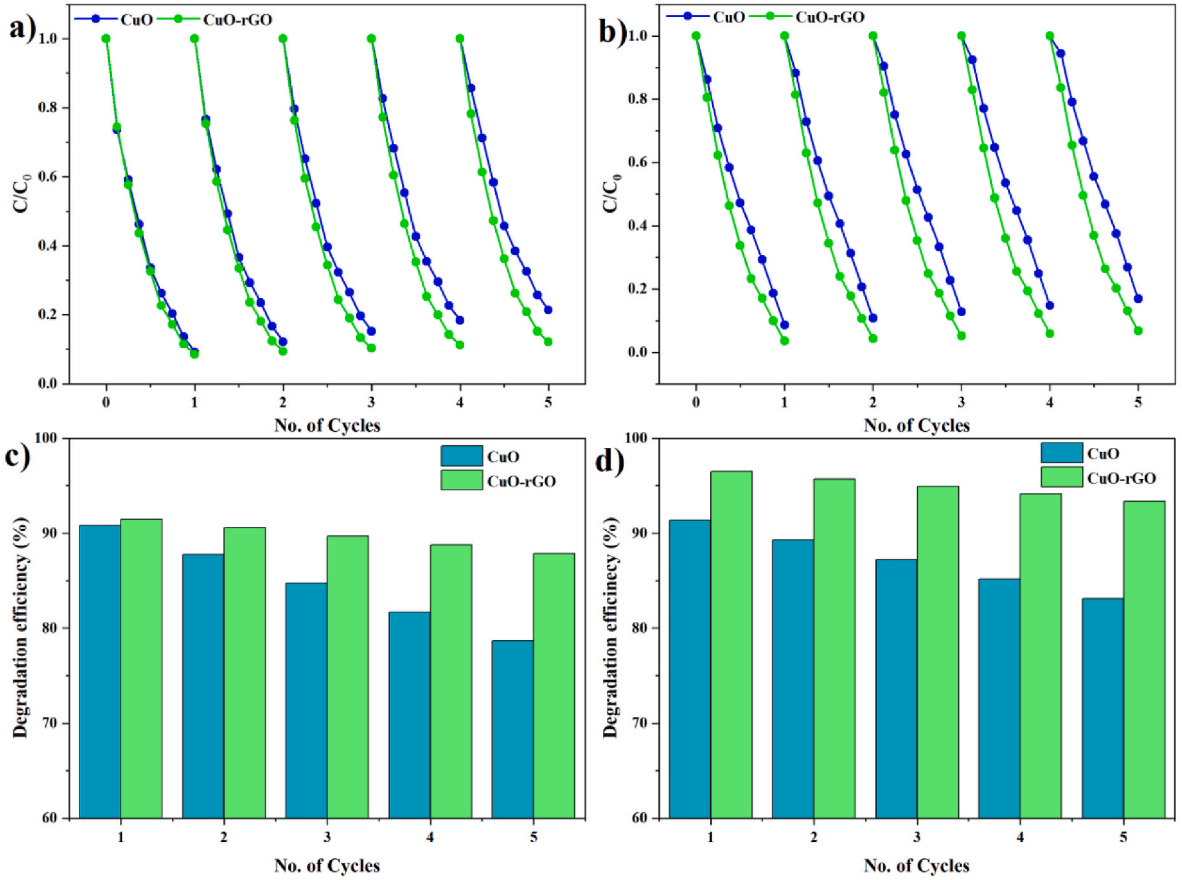


Fig. 13. Cyclic degradation of prepared CuO and CuO-rGO nanocomposite, C/C_0 curve for a) RB, b)Rh6G, and degradation efficiency towards c) RB and d) Rh6G.

Conceptualization, Data curation, Formal analysis, Software. **C. Shanthi:** Formal analysis, Funding acquisition, Resources, Validation. **A. Panneerselvam:** Formal analysis, Resources, Software, Validation, Writing – review & editing. **S. Senthilkumar:** Data curation, Formal analysis, Writing – review & editing. **B.V. Bhuvaneswari:** Data curation, Investigation, Validation, Writing – review & editing.

Consent to publish

Not applicable.

Ethics approval and consent to participate

Not applicable.

Availability of data and materials

The datasets used or analyzed during the current study are available from the corresponding author upon reasonable request.

Declaration of competing interest

The authors declare no competing financial interests.

Acknowledgment

The authors acknowledge the research facilities like UV–Vis spectrophotometer and Fluorescence Spectrophotometer provided by the Board of Research and Nuclear Science (BRNS), Mumbai (Sanction no: 2013/34/30/BRNS/1127 dt.September 19, 2013) to conduct this research work. Authors also thank DST-Fund for Improvement of Science and Technology (DST-FIST) to our research centre [Vide FIST No. 368 dt. January 14, 2016].

References

[1] V. Kavitha, P. Mahalingam, M. Jeyanthinath, N. Sethupathi, Optical and structural properties of tungsten-doped barium strontium titanate, in: Proceedings of the Materials Today: Proceedings, 23, 2019.
[2] V. Kavitha, J. Mayandi, P. Mahalingam, N. Structural Sethupathi, Optical and electrical studies on zinc doped barium strontium titanate as photo-anode for DSSC device, in: Proceedings of the Materials Today: Proceedings, 35, 2019.
[3] S.A. Akintelu, A.S. Folorunso, F.A. Folorunso, A.K. Oyebamiji, Green synthesis of copper oxide nanoparticles for biomedical application and environmental remediation, Heliyon 6 (2020) e04508.
[4] T.B. Vidovix, H.B. Quesada, E.F.D. Januário, R. Bergamasco, A.M.S. Vieira, Green synthesis of copper oxide nanoparticles using punica granatum leaf extract applied to the removal of methylene blue, Mater. Lett. 257 (2019), https://doi.org/10.1016/j.matlet.2019.126685.
[5] S. Vasantharaj, S. Sathiyavimal, P. Senthilkumar, V.N. Kalpana, G. Rajalakshmi, M. Alsehli, A. Elfasakhany, A. Pugazhendhi, Enhanced photocatalytic degradation of water pollutants using bio-green synthesis of zinc oxide nanoparticles (ZnO NPs), J. Environ. Chem. Eng. 9 (2021), https://doi.org/10.1016/j.jece.2021.105772.
[6] B. Djamila, L.S. Eddine, B. Abderrhmane, A. Nassiba, A. Barhoum, In vitro antioxidant activities of copper mixed oxide (CuO/Cu2O) nanoparticles produced from the leaves of Phoenix dactylifera L, Biomass Convers Biorefin 14 (2024) 6567–6580, https://doi.org/10.1007/s13399-022-02743-3.
[7] M.L. Ben Amor, S. Zeghdi, S.E. Laouini, A. Bouafia, S. Meneceur, PH reaction effect on biosynthesis of CuO/Cu $_2$ O nanoparticles by moringa oleifera leaves extracts for antioxidant activities, Inorganic and Nano-Metal Chemistry 53 (2023) 437–447, https://doi.org/10.1080/24701556.2022.2077376.
[8] S. Legmairi, S. Meneceur, G.G. Hasan, L.S. Eddine, H.A. Mohammed, F. Alharthi, J. A.A. Abdullah, Enhanced photocatalytic activity and antiviral evaluation of CuO@ Fe $_2$ O $_3$ NC for amoxicillin degradation and SARS-CoV-2 treatment, Nanotechnology 34 (2023) 445101, https://doi.org/10.1088/1361-6528/acebfa.
[9] A. Serouti, L.S. Eddine, S. Meneceur, G.G. Hasan, H.A. Mohammed, C. Salmi, K. Iman, M.F. Ferhat, O. Ben Ali, J.A.A. Abdullah, Biogenic ZnO/CuO/Fe2O3 nanocomposite: a groundbreaking approach for enhanced degradation capabilities and reusability in dye removal applications, Arab J Sci Eng 49 (2024) 753–764, https://doi.org/10.1007/s13369-023-08495-0.
[10] S. Sathiyavimal, S. Vasantharaj, V. Veeramani, M. Saravanan, G. Rajalakshmi, T. Kaliannan, F.A. Al-Misned, A. Pugazhendhi, Green chemistry route of biosynthesized copper oxide nanoparticles using psidium guajava leaf extract and their antibacterial activity and effective removal of industrial dyes, J. Environ. Chem. Eng. 9 (2021), https://doi.org/10.1016/j.jece.2021.105033.
[11] S. Sakthinathan, T. Kokulnathan, S.-M. Chen, R. Karthik, P. Tamizhdurai, T.-W. Chiu, K. Shanthi, Simple sonochemical synthesis of cupric oxide sphere decorated reduced graphene oxide composite for the electrochemical detection of flutamide drug in biological samples, J. Electrochem. Soc. 166 (2019), https://doi.org/10.1149/2.0561902jes.
[12] R. sayyad, M. Ghambari, T. Ebadzadeh, A.H. Pakseresht, E. Ghasali, Preparation of Ag/reduced graphene oxide reinforced copper matrix composites through spark plasma sintering: an investigation of microstructure and mechanical properties, Ceram. Int. 46 (2020), https://doi.org/10.1016/j.ceramint.2020.02.142.
[13] M. Sudha, S. Surendhiran, V. Gowthambabu, A. Balamurugan, R. Anandarasu, Y. A. Syed Khadar, D. Vasudevan, Enhancement of corrosive-resistant behavior of Zn and Mg metal plates using biosynthesized nickel oxide nanoparticles, J Bio Tribocorros 7 (2021) 60, https://doi.org/10.1007/s40735-021-00492-w.
[14] K. Kandasamy, S. Surendhiran, K.S.G. Jagan, G.S. Kumar, Y.A.S. Khadar, P. Rajasingh, Green synthesis of CdS quantum dots for photocatalytic and anti-corrosive applications in aqueous media, Applied Surface Science Advances 13 (2023) 100364, https://doi.org/10.1016/j.apsadv.2022.100364.
[15] D.A. Kospa, A.I. Ahmed, S.E. Samra, A.A. Ibrahim, High efficiency solar desalination and dye retention of plasmonic/reduced graphene oxide based copper oxide nanocomposites, RSC Adv. 11 (2021), https://doi.org/10.1039/d1ra01663f.
[16] T. Pisarkiewicz, W. Maziarz, A. Małolepszy, L. Stobiński, D. Michoń, A. Rydosz, Multilayer structure of reduced graphene oxide and copper oxide as a gas sensor, Coatings 10 (2020), https://doi.org/10.3390/coatings10111015.
[17] S. Pourbeyram, J. Abdollahpour, M. Soltanpour, Green synthesis of copper oxide nanoparticles decorated reduced graphene oxide for high sensitive detection of glucose, Mater. Sci. Eng. C 94 (2019), https://doi.org/10.1016/j.msec.2018.10.034.
[18] L. Li, L. Dong, W. Huo, W. Zhang, Y. Liu, J.A. Lu, Simple approach to obtaining enhanced mechanical properties of graphene/copper composites with heterogeneous grain structures, Mater. Sci. Eng., A 832 (2022), https://doi.org/10.1016/j.msea.2021.142438.
[19] S.E. Elugoke, O.E. Fayemi, A.S. Adekunle, B.B. Mamba, T.T.I. Nkambule, E. E. Ebenso, Electrochemical sensor for the detection of dopamine using carbon quantum dots/copper oxide nanocomposite modified electrode, FlatChem 33 (2022), https://doi.org/10.1016/j.flatc.2022.100372.
[20] Z. Xiang, X. Wang, L. Xu, Z. Wang, J. Meng, J. Zhang, J. Zhao, H. Wang, Synthesis of cuprous oxide nanoparticles on graphitic carbon nitride and reduced graphene oxide and their catalytic performance toward the reduction of 4-nitrophenol, J. Mater. Sci. 57 (2022), https://doi.org/10.1007/s10853-021-06771-8.
[21] A. Singh, A. Sharma, A. Ahmed, S. Arya, Highly selective and efficient electrochemical sensing of ascorbic acid via CuO/RGO nanocomposites deposited on conductive fabric, Appl. Phys. Mater. Sci. Process 128 (2022), https://doi.org/10.1007/s00339-022-05436-w.
[22] S. Surendhiran, V. Gowthambabu, A. Balamurugan, M. Sudha, V.B. Senthil Kumar, K.C. Suresh, Rapid green synthesis of CuO nanoparticles and evaluation of its photocatalytic and electrochemical corrosion inhibition performance, in: Proceedings of the Materials Today: Proceedings, 47, 2021.
[23] V. Devabharathi, K.S.G. Jagan, S.R. Priyan, T.N. Vidaarth, S. Surendhiran, Y.A. S. Khadar, K. Kandasamy, Rational design of NiO nanoflakes and porous GCN nanocomposite for synergic effectiveness on photocatalytic degradation of industry effluents and biological activity, Chemical Physics Impact 8 (2024), https://doi.org/10.1016/j.chphi.2024.100637.
[24] I. Kir, H.A. Mohammed, S.E. Laouini, M. Souhaila, G.G. Hasan, J.A.A. Abdullah, S. Mokni, A. Naseef, A. Alsalme, A. Barhoum, Plant extract-mediated synthesis of CuO nanoparticles from lemon peel extract and their modification with polyethylene glycol for enhancing photocatalytic and antioxidant activities, J. Polym. Environ. 32 (2024) 718–734, https://doi.org/10.1007/s10924-023-02976-x.
[25] K. Andrade-Zavaleta, Y. Chacon-Laiza, D. Asmat-Campos, N. Raquel-Checca, Green synthesis of superparamagnetic iron oxide nanoparticles with Eucalyptus globulus extract and their application in the removal of heavy metals from agricultural soil, Molecules 27 (2022), https://doi.org/10.3390/molecules27041367.
[26] M.U. Sadiq, A. Shah, A. Haleem, S.M. Shah, I. Shah, Eucalyptus globulus mediated green synthesis of environmentally benign metal based nanostructures: a review, Nanomaterials 13 (2023).
[27] P. Salgado, D.O. Mártire, G. Vidal, Eucalyptus extracts-mediated synthesis of metallic and metal oxide nanoparticles: current status and perspectives, Mater. Res. Express 6 (2019).
[28] T.M. Thakur, R.S. Lokhande, M.M. Thigle, V.R. Patil, Nanoparticles of chromium oxide by green synthesis using Eucalyptus globulous leaves extract; characterization and biological activity studies, in: Proceedings of the Materials Today: Proceedings, 79, 2022.
[29] X. Weng, X. Jin, J. Lin, R. Naidu, Z. Chen, Removal of mixed contaminants Cr(VI) and Cu(II) by green synthesized iron based nanoparticles, Ecol. Eng. 97 (2016), https://doi.org/10.1016/j.ecoleng.2016.08.003.
[30] K. Wang, Y. Liu, X. Jin, Z. Chen, Characterization of iron nanoparticles/reduced graphene oxide composites synthesized by one step Eucalyptus leaf extract, Environ. Pollut. 250 (2019), https://doi.org/10.1016/j.envpol.2019.04.002.
[31] H. Bakdi, N. Lenchi, S. Kebbouche-Gana, N.E. Djelali, Obtention of green-synthesized silver nanoparticles and evaluation of its antimicrobial and antifungal activity against skin pathogenic microorganisms, Biotecnol. Apl. 39 (2022).
[32] DrM.B. Vanarotti, DrC.P. Jawahar, Green synthesis of zinc oxide nanoparticles using Eucalyptus lanceolata leaf litter in the control of bacterial and fungal crop diseases, Mig. Let. 20 (2023), https://doi.org/10.59670/ml.v20is13.6287.

[33] P. Narasaiah, B.K. Mandal, N.C. Sarada, Biosynthesis of copper oxide nanoparticles from Drypetes sepiaria leaf extract and their catalytic activity to dye degradation, in: Proceedings of the IOP Conference Series: Materials Science and Engineering, 263, 2017.
[34] W. Saeed, Z. Abbasi, S. Majeed, S.A. Shahzad, A.F. Khan, A.J. Shaikh, An insight into the binding behavior of graphene oxide and noble metal nanoparticles, J. Appl. Phys. 129 (2021), https://doi.org/10.1063/5.0041894.
[35] M. Kalaiyarasi, M. Nivedha, M. Mani, R. Harikrishnan, J.K. Kumar, S. Loganathan, K. Kaviyarasu, Synthesis of CuO/NaCuSO4 nanocomposite using an aqueous extract of tribulus terrestris and their structural, optical, morphology and dielectric studies, Chem. Pap. 78 (2024), https://doi.org/10.1007/s11696-023-03294-1.
[36] A.S. Sathishkumar, K.A. Balasubramanian, T. Ramkumar, Structural characterization of ZnO, CuO and Fe2O3 nanoparticles: evaluation of Rietveld refinement, Tierarztl. Prax. 40 (2020).
[37] A.A. Yadav, Y.M. Hunge, S.W. Kang, Spongy ball-like copper oxide nanostructure modified by reduced graphene oxide for enhanced photocatalytic hydrogen production, Mater. Res. Bull. 133 (2021), https://doi.org/10.1016/j.materresbull.2020.111026.
[38] W. Bai, M. Wu, X. Du, W. Gong, Y. Ding, C. Song, L. Liu, Synergistic effect of multiple-phase RGO/CuO/Cu2O heterostructures for boosting photocatalytic activity and durability, Appl. Surf. Sci. 544 (2021), https://doi.org/10.1016/j.apsusc.2020.148607.
[39] M. Strankowski, D. Włodarczyk, Ł. Piszczyk, J. Strankowska, Polyurethane nanocomposites containing reduced graphene oxide, FTIR, Raman, and XRD studies, Journal of Spectroscopy 2016 (2016), https://doi.org/10.1155/2016/7520741.
[40] M.A. Hosseini, S. Malekie, N. Ebrahimi, The analysis of linear dose-responses in gamma-irradiated graphene oxide: can FTIR analysis Be considered a novel approach to examining the linear dose-responses in carbon nanostructures? Radiat. Phys. Chem. 176 (2020) https://doi.org/10.1016/j.radphyschem.2020.109067.
[41] P.K. Singh, Thermogravimetric analysis and FTIR analysis of electrochemically synthesized graphene oxide (GO)/Reduced graphene oxide (RGO), IOP Conf. Ser. Mater. Sci. Eng. 1116 (2021), https://doi.org/10.1088/1757-899x/1116/1/012003.
[42] G. Williams, B. Seger, P.V. Kamt, TiO2-Graphene nanocomposites. UV-assisted photocatalytic reduction of graphene oxide, ACS Nano 2 (2008), https://doi.org/10.1021/nn800251f.
[43] G. Park, D. Go, S. Jo, T.H. Lee, J.W. Shin, J. An, High-performance graphene-dielectric interface by UV-assisted atomic layer deposition for graphene field effect transistor, Adv Electron Mater 9 (2023), https://doi.org/10.1002/aelm.202300074.
[44] L. Kuo, B.J. Luijten, S. Li, A.C.M. De Moraes, A.J. Silvaroli, S.G. Wallace, J. Hui, J. R. Downing, K.R. Shull, M.C. Hersam, Sterilizable and reusable UV-resistant graphene-polyurethane elastomer composites, ACS Appl. Mater. Interfaces 14 (2022), https://doi.org/10.1021/acsami.2c17791.
[45] S.I. Shin, A. Go, I.Y. Kim, J.M. Lee, Y. Lee, S.J. Hwang, A beneficial role of exfoliated layered metal oxide nanosheets in optimizing the electrocatalytic activity and pore structure of Pt-reduced graphene oxide nanocomposites, Energy Environ. Sci. 6 (2013), https://doi.org/10.1039/c2ee22739h.
[46] P. Van Tuan, H.B. Tuong, V.T. Tan, L.H. Thu, N.D. Khoang, T.N. Khiem, SnO2/Reduced graphene oxide nanocomposites for highly efficient photocatalytic degradation of methylene blue, Opt. Mater. 123 (2022), https://doi.org/10.1016/j.optmat.2021.111916.
[47] S. Karthikeyan, K. Dhanakodi, S. Surendhiran, K.S.G. Jagan, N. Lenin, L. Dhatchinamurthy, A.T. Rajamanickam, Sonochemical synthesis of Sn-doped La2O3 nanoparticles and its for the photocatalytic degradation of hazardous, J. Mater. Sci. Mater. Electron. 34 (2023) 1157.
[48] S. Karthikeyan, K. Dhanakodi, S. Surendhiran, K.S.G. Jagan, P. Thirunavukkarasu, L. Arunraja, Effect of synthesis parameters on the structural, morphological, and photocatalytic activity of La2O3, J. Indian Chem. Soc. 100 (2023) 100860.
[49] G. Zhu, X. Li, H. Wang, L. Zhang, Microwave assisted synthesis of reduced graphene oxide incorporated MOF-derived ZnO composites for photocatalytic application, Catal. Commun. 88 (2017), https://doi.org/10.1016/j.catcom.2016.09.024.
[50] J. Yang, X. Wang, X. Zhao, J. Dai, S. Mo, Synthesis of uniform Bi2WO6-reduced graphene oxide nanocomposites with significantly enhanced photocatalytic reduction activity, J. Phys. Chem. C 119 (2015) 3068–3078, https://doi.org/10.1021/JP510041X.
[51] J. Qiu, P. Zhang, M. Ling, S. Li, P. Liu, H. Zhao, S. Zhang, Photocatalytic synthesis of TiO 2 and reduced graphene oxide nanocomposite for lithium ion battery, ACS Appl. Mater. Interfaces 4 (2012) 3636–3642, https://doi.org/10.1021/AM300722D.
[52] Y. Sang, Z. Zhao, J. Tian, P. Hao, H. Jiang, H. Liu, J.P. Claverie, Enhanced photocatalytic property of educed graphene oxide/TiO 2 nanobelt surface heterostructures constructed by an in situ photochemical reduction method, Small 10 (2014) 3775–3782, https://doi.org/10.1002/SMLL.201303489.
[53] A. Iwase, Y. Ng, Y. Ishiguro, A.K.-J. of the A., Undefined reduced graphene oxide as a solid-state electron mediator in Z-scheme photocatalytic water splitting under visible light, ACS Publications 133 (2011) 11054–11057, https://doi.org/10.1021/ja203296z, 2011.
[54] G. Ali, S. Jazib Abbas Zaidi, M. Abdul Basit, T.J. Park, Synergetic performance of systematically designed G-C3N4/RGO/SnO2 nanocomposite for photodegradation of rhodamine-B dye, Appl. Surf. Sci. 570 (2021), https://doi.org/10.1016/j.apsusc.2021.151140.
[55] S.M. Botsa, G.P. Naidu, M. Ravichandra, S.J. Rani, R.B. Anjaneyulu, C.V. Ramana, Flower like SnO2-Fe2O3-RGO ternary composite as highly efficient visible light induced photocatalyst for the degradation of organic pollutants from contaminated water, J. Mater. Res. Technol. 9 (2020), https://doi.org/10.1016/j.jmrt.2020.08.087.
[56] M. Najjar, H.A. Hosseini, A. Masoudi, Z. Sabouri, A. Mostafapour, M. Khatami, M. Darroudi, Green chemical approach for the synthesis of SnO2 nanoparticles and its application in photocatalytic degradation of eriochrome black T dye, Optik 242 (2021) 167152, https://doi.org/10.1016/j.ijleo.2021.167152.
[57] M. Golmohammadi, M.N. Hassankiadeh, L. Zhang, Facile biosynthesis of SnO2/ZnO nanocomposite using acroptilon repens flower extract and evaluation of their photocatalytic activity, Ceram. Int. 47 (2021), https://doi.org/10.1016/j.ceramint.2021.07.095.
[58] A.S. Manjunatha, N.S. Pavithra, M. Shivanna, G. Nagaraju, C.R. Ravikumar, Synthesis of citrus limon mediated SnO2-WO3nanocomposite: applications to photocatalytic activity and electrochemical sensor, J. Environ. Chem. Eng. 8 (2020), https://doi.org/10.1016/j.jece.2020.104500.
[59] T. Vijayaraghavan, R. Althaf, P. Babu, K.M. Parida, S. Vadivel, A.M. Ashok, Visible light active LaFeO3 nano perovskite-RGO-NiO composite for efficient H2 evolution by photocatalytic water splitting and textile dye degradation, J. Environ. Chem. Eng. 9 (2021), https://doi.org/10.1016/j.jece.2020.104675.
[60] H. Alijani, M. Abdouss, H. Khataei, Efficient photocatalytic degradation of toxic dyes over BiFeO3/CdS/RGO nanocomposite under visible light irradiation, Diam. Relat. Mater. 122 (2022), https://doi.org/10.1016/j.diamond.2021.108817.